Structural, electronic, and optical properties of quaternary alloys $Al_{0.50}Ga_{0.50}N_xSb_{1-x}$: a first-principles study

M. Berber[a,b,*], N. Bouzouira[a,c], M. Mebrek[a,b], A. Boudali[d], H. Abid[e], and H. Moujri[e]

[a]*Centre Universitaire Nour Bachir El Bayadh, 32000 El Bayadh, Algérie*
e-mail: berbermohamed@yahoo.fr
[b]*Laboratoire d'Instrumentation et Matériaux Avancés,*
Centre Universitaire Nour Bachir El-Bayadh, BP 900 route Aflou, 32000, Algérie
[c]*Laboratory of Physical Chemistry of Advanced Materials,*
University of Djillali Liabes, BP 89, Sidi-Bel-Abbes 22000, Algeria.
[d]*Laboratory of Physico-chemical Studies, University of Saida, Algeria.*
[e]*Applied Materials Laboratory, Research Center,*
Sidi Bel Abbès Djillali Liabes University, 22000, Algeria
[f]*Renewable Energy Laboratory and dynamic systems,*
Faculté des Sciences Ain-Chock, Université Hassan II de Casablanca, Morocco.

In this study, we have employed the first-principle methods based on density functional theory to investigate the structural, electronic, and optical properties of $Al_{0.50}Ga_{0.50}N_xSb_{1-x}$ in zincblende structure. The exchange and correlation potential is described by the generalized gradient approximation of Perdew, Burke, and Ernzerhof (GGA-PBEsol) coupled with TB-mBJ approaches. The studied structures show that all structures are semiconductors and have a direct bandgap except $Al_{0.50}Ga_{0.50}N_{0.25}Sb_{0.75}$, which has a semi-metallic behavior. The optical properties such as refractive index, extinction coefficient, and optical conductivity are discussed in detail. Our result shows these materials are considered as promising materials for optoelectronic applications in the visible and infrared region. To our knowledge, this is the first time that a study has been done on this alloy, and we would like it to serve as a reference for the next studies.

1. Introduction

The admixture of various chemical elements such as group III-V and group II-VI is used to control different physical properties of semiconductors, primarily the lattice constant, the amplitude of the bandgap, and, consequently, the optoelectronic properties, to fulfill the requirement for a specific function of semiconductor compounds. Such possibilities are reached thanks to the development of ternary alloys, but the researchers want to refine and expand their applications, thanks to the development of ternary alloys such perspectives are achieved, but the researchers want to refine and extend their applications, this perspective has been realized by the formation of four elements (quaternary alloy). The ability of quaternary alloys formation accesses further research lines and performs an improved technique to better change distinct semiconductor physical properties. Group IIIA-VA semiconductors including GaAs, AlP, GaN, GaSb, InP, InAs, and InSb are popular binary alloys for microelectronic and optoelectronic use. The application of quaternary layers based on these binary alloys to the material design again gives greater versatility to adjust the band distance and band offsets of matched InP or GaAs lattice heterostructures [1-4]. Many theoretical and experimental studies on quaternary alloys for use in various fields have recently been carried out. Hosni and colleagues have presented a comparative analysis and found that the large optical gain and wavelength for fiber optic communications can be obtained by applying AlGaInAs quaternary nanowires [5]. Another research carried out by Yingxin *et al*. indicates the positive growth of $In_{1-x}Ga_xAs_{1-y}Bi_y$ in the metal-organic vapor phase epitaxy (MOVPE) on the InP substrate [6]. The surface morphology of $InAs_{1-x-y}Sb_xP_y$ epilayers grown by liquid phase epitaxy has been studied. The study shows that globules and hillocks have no effects on the crystalline quality and compositional uniformity of $InAs_{1-x-y}Sb_xP_y$ epilayers [7]. Our research theory is based on predicting the structural, electronic and optical properties of alloys with various N concentrations x (0.125, 0.25, 0.75, and 0.875) in $Al_{0.50}Ga_{0.50}N_xSb_{1-x}$. We have employed in this prediction the full-potential linearized augmented plane wave (FP-LAPW) method within density functional theory (DFT) [8]. We studied the effect of the quaternary $Al_{0.50}Ga_{0.50}N_xSb_{1-x}$ concentration of nitrogen atoms on the structural, electronic, and optical properties. Following our library search and according to our knowledge, there is neither theoretical nor experimental data about $Al_{0.50}Ga_{0.50}N_xSb_{1-x}$ for comparison.

This article is structured as follows, after the abstract and introduction. In Sec. 2 of this paper establish a short description of the computational method used in this study. A

detailed description of the acquired results and their interpretation related to structural, electronic and optical properties of Al$_{0.50}$Ga$_{0.50}$N$_x$Sb$_{1-x}$ alloys are presented in Sec. 3.

2. Calculation details

The WIEN2k code [9-11] has been used to explore first-principles investigations. In this paper, the effect of exchange-correlation in the GGA was evaluated within Perdew-Burke-Ernzerhof (PBE) [12] potential. It is acknowledged that the standard semi-local GGA undervalues band gaps; for that reason, we have completed the exchange and correlation effects of self-consistency by using the modified Becke-Johnson (mBJ) potential [13]. This approximation is a modified version of the Becke-Johnson potential employed to ameliorate band gaps obtained by the conventional density functional theory (DFT) based methods. The mBJ exchange-correlation potential has importantly improved band gap results for wide bandgap insulators and doped semiconductor structures [13-21].

In this work, we have selected the following calculation parameters: the muffin-tin radii (MT) for Al, Ga, N, and Sb to be 2.0, 2.20, 1.8, and 2.50 atomic units (a.u.), respectively. The $K_{\max} = 9$ (RMT)$^{-1}$ ($K_{\max}$ is the plane wave cut-off and RMT is the smallest of all atomic sphere radii). The Fourier expanded charge density was truncated at $G_{\max} = 12$(Ryd)$^{1/2}$, the $l-$expansion of the non-spherical potential and charge density was carried out up to $l_{\max} = 10$. The cut-off energy is set to -6 Ryd to separate the core from valence states. The self-consistent calculations are judged to be converged when the total energy of the system is stable within 0.0001 Ryd.

To predict the structural, electronic, and optical properties of the Al$_{0.50}$Ga$_{0.50}$N$_x$Sb$_{1-x}$ quaternary alloys, we have employed a $(2 \times 2 \times 2)$ supercell with 16 atoms, 8 atoms for the group III (Aluminum (Al) and Gallium (Ga)), and 8 atoms for group VI (Azote (N) and Antimonide (Sb)). We have chosen 4 atoms for Aluminum and 4 atoms for Gallium to create the structure Al$_{0.50}$Ga$_{0.50}$N$_x$Sb$_{1-x}$. To build the structure Al$_{0.50}$Ga$_{0.50}$N$_{0.125}$Sb$_{0.875}$, Al$_{0.50}$Ga$_{0.50}$N$_{0.25}$Sb$_{0.75}$, Al$_{0.50}$Ga$_{0.50}$N$_{0.75}$Sb$_{0.25}$, and Al$_{0.50}$Ga$_{0.50}$N$_{0.875}$Sb$_{0.125}$, we have chosen 1, 2, 6, and 7 atoms for N, respectively. We note that all structures have a cubic structure in space group F-43m (no.216) (zincblende). The electronic configurations of Al, Ga, N, and Sb are Al: [Ne] 3s^{2}3p^1, Ga: [Ar] 3d^{10}4s^{2}4p^1, N: [He] 2s^{2}2p^3 and Sb: [Kr] 4d^{10}5s^{2}5p^3.

3. Results and discussions

3.1. Structural properties

To predict the ground state properties such as the equilibrium lattice constant a, the bulk modulus B_0 and the bulk modulus pressure derivative B', we have optimized all structures Al$_{0.50}$Ga$_{0.50}$N$_x$Sb$_{1-x}$ with ($x = 0.125, 0.25, 0.75, 0.875$), and we have calculated the total energies, according to the

unit cell volumes and fitted to the Birch-Murnaghan's equation of state (EOS) [22] and it's based necessarily on two parameters: the compressibility B_0 and its first derivative B_0' with respect to the pressure. These two constants are resolved by adapting the energy versus the volume; the isothermal compressibility modulus B is related to the curvature of the function $E(V)$ by the following relation:

$$E(V) = E_0 + B_0 V_0 \left[\frac{1}{B_0' - 1} \left(\frac{V_0}{V} \right)^{B_0' - 1} + \frac{1}{B_0' V_0} - \frac{1}{B_0' - 1} \right] \qquad (1)$$

With V_0, E_0, B_0, and B_0' are the volume, total energy, compressibility modulus, and its first derivative, respectively. The studied structural parameters of Al$_{0.50}$Ga$_{0.50}$N$_x$Sb$_{1-x}$ for various concentrations are resumed in Table I, together with the available theoretical and experimental data. Figure 1 exhibit the variation of parameter lattice a as a function of the composition (x) for Al$_{0.50}$Ga$_{0.50}$N$_x$Sb$_{1-x}$, the linear liaison between the parameter lattice and Nitrogen (N) concentration x is calculated by Vegard's law [23] as follows:

$$a(x) = 6.20511 - 1.56933x. \qquad (2)$$

Generally, the relation between the parameter lattice and concentration is not always linear, for that we have to use the quadratic relationship obtained by fitting:

$$a(x) = 6.07398 - 041905x - 1.13664x^2. \qquad (3)$$

Equation (4) represents the quadratic relation of bulk modulus as a function of the concentration x.

$$B(x) = 62.47267 - 64.14484x + 149.56032x^2. \qquad (4)$$

Figure 2 exhibit the calculated bulk modus as a function of concentration x.

Equation	y = Intercept + B1*x^1 + B2 *x^2
Plot	a
Weight	No Weighting
Intercept	6.07398 ± 0.02759
B1	-0.41905 ± 0.16818
B2	-1.13664 ± 0.16693
Residual Sum of Square	1.70087E-4
R-Square (COD)	0.99983
Adj. R-Square	0.99949
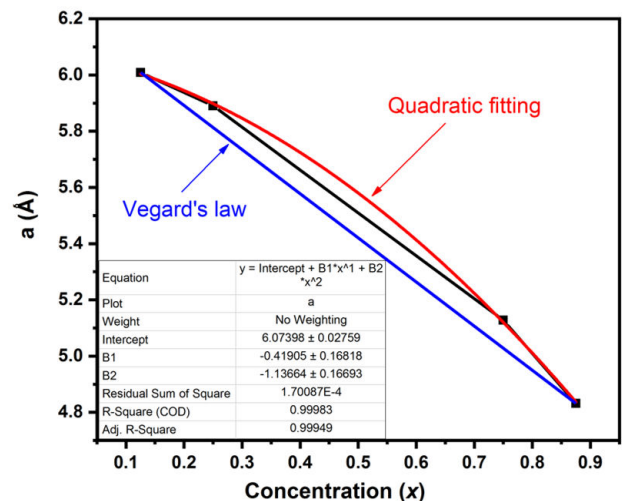
FIGURE 1. Calculated lattice constant a of Al$_{0.50}$Ga$_{0.50}$N$_x$Sb$_{1-x}$ as a function of concentration (x).
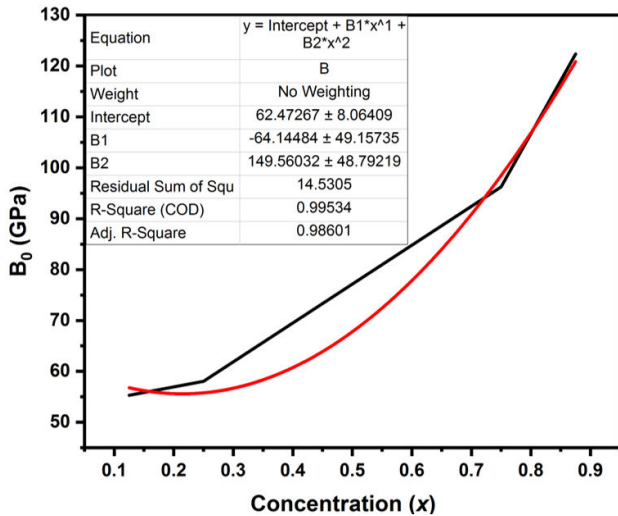
FIGURE 2. Calculated bulk modulus B_0 of $Al_{0.50}Ga_{0.50}N_xSb_{1-x}$ as a function of concentration (x).

TABLE I. Calculated lattice constant (a), bulk modulus (B) for $Al_{0.50}Ga_{0.50}N_xSb_{1-x}$ at concentrations $x = 0.125, 0.25, 0.75$, and 0.875.

Compound	$a(Å)$	$B(GPa)$
$Al_{0.50}Ga_{0.50}N_{0.25}Sb_{0.875}$	6.00895	55.2963
$Al_{0.50}Ga_{0.50}N_{0.25}Sb_{0.75}$	5.89050	58.0267
$Al_{0.50}Ga_{0.50}N_{0.75}Sb_{0.25}$	5.12800	96.2490
$Al_{0.50}Ga_{0.50}N_{0.875}Sb_{0.125}$	4.83195	122.3482

3.2. Electronic properties

In this part, to predict and know the nature of the bandgap, we have calculated the electronic band structure for $Al_{0.50}Ga_{0.50}N_xSb_{1-x}$ with different concentration x ($x = 0.125, 0.25, 0.75, 0.875$) using GGA-PBEsol [12] jointed
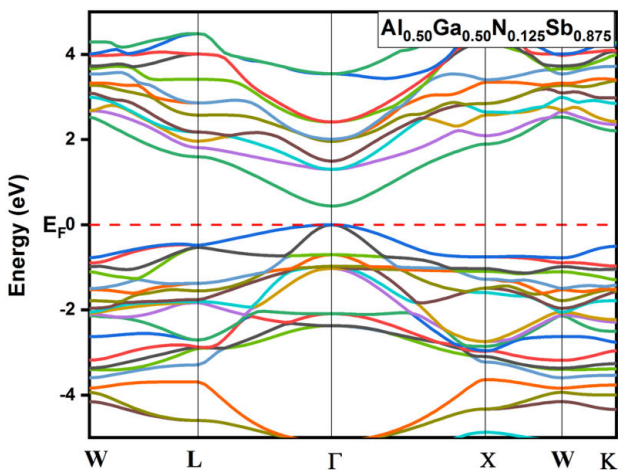
FIGURE 3. Electronic band structures for $Al_{0.50}Ga_{0.50}N_{0.125}Sb_{0.875}$ using GGA-PBEsol and TB-mBJ approximation.
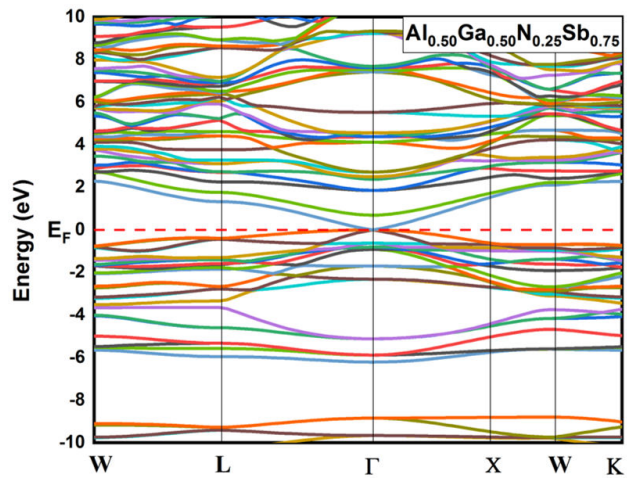
FIGURE 4. Electronic band structures for $Al_{0.50}Ga_{0.50}N_{0.25}Sb_{0.75}$ using GGA-PBEsol and TB-mBJ approximation.
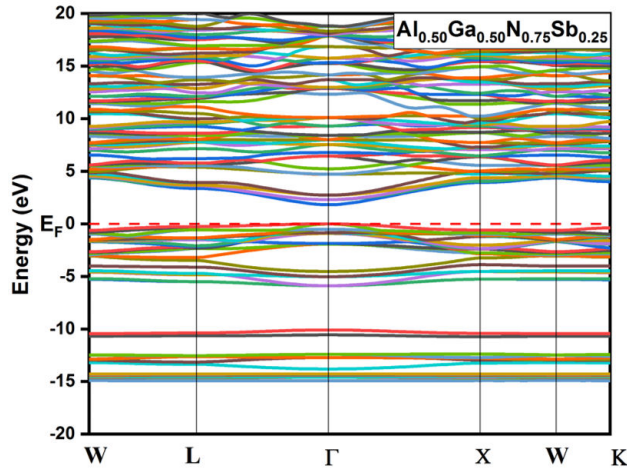
FIGURE 5. Electronic band structures for $Al_{0.50}Ga_{0.50}N_{0.75}Sb_{0.25}$ using GGA-PBEsol and TB-mBJ approximation.

with (TB-mBJ) of Tran-Blaha modified Becke-Johnson approximation. The band structure is an indispensable aspect to explore the electronic properties of solids. An important element of details given by the band structure is the width of the energy bandgap (Eg), which is the energy separating the valence band top to the conduction band bottom. The calculated structures along the high symmetry directions of $Al_{0.50}Ga_{0.50}N_xSb_{1-x}$ alloys for $x = 0.125, 0.25, 0.75$ and 0.875 are given in Fig. 3, 4, 5, and 6, respectively. The top of the valence band and the bottom of the conduction band are located at $\Gamma - \Gamma$ high-symmetry points and give a direct band for all structures, except for $Al_{0.50}Ga_{0.50}N_{0.25}Sb_{0.75}$, an alloy which has a zero bandgap and which has semi-metallic behavior [24,25]. The calculated $Al_{0.50}Ga_{0.50}N_xSb_{1-x}$ band gaps using GGA-PBEsol and TB-mBJ approximation, with available experimental theoretical data, are listed in Table II. Figure 7 shows the deviation of band gap energies Eg of $Al_{0.50}Ga_{0.50}N_xSb_{1-x}$ in relation with N concentration (x).
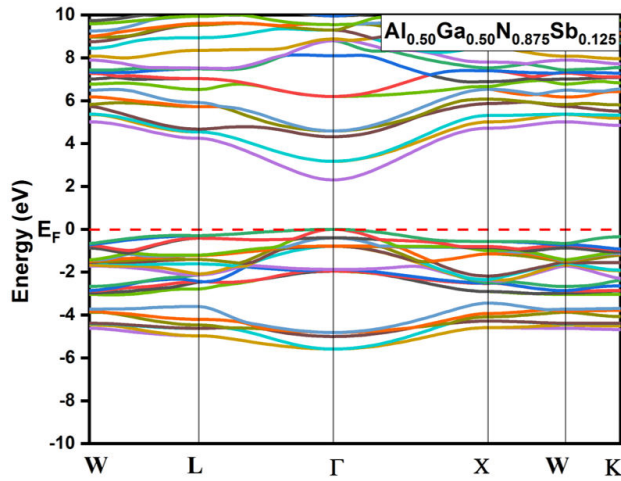
FIGURE 6. Electronic band structures for Al$_{0.50}$Ga$_{0.50}$N$_{0.875}$Sb$_{0.125}$ using GGA-PBEsol and TB-mBJ approximation.
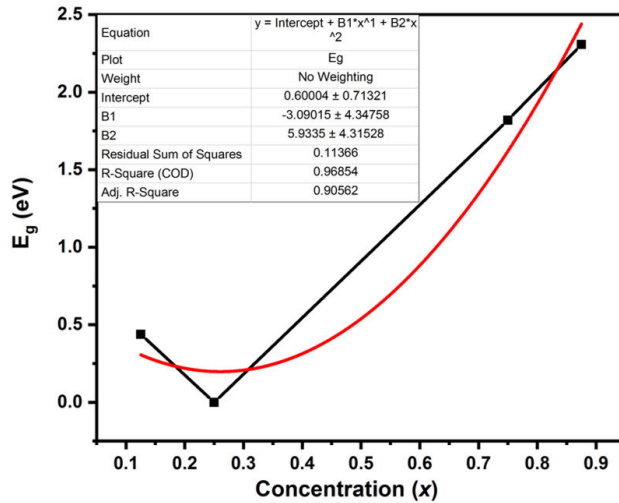
FIGURE 7. The variation of band gap energies E_g of Al$_{0.50}$Ga$_{0.50}$N$_x$Sb$_{1-x}$ as a function of N concentration (x).

3.3. Optical properties

The study done by Ehrenreich and Cohen will allow us to describe the dielectric function as a complex function as:

$$\varepsilon(\omega) = \varepsilon_1(\omega) + i\varepsilon_2(\omega), \tag{5}$$

where $\varepsilon_1(\omega)$ and $\varepsilon_2(\omega)$ are the real and the imaginary parts of the dielectric function, respectively. This frequency-dependent complex dielectric function is known to describe the optical response of the medium at all phonon energies $E = \hbar\omega$. The imaginary part of the $\varepsilon(\omega)$ in the long-wavelength limit has been collected directly from the electronic structure calculation, using the joint density of states (JDOS) and the transition moments elements $M_{cv}(k)$:

$$\varepsilon_2(\omega) = \frac{4\pi e^2}{\Omega\varepsilon_0} \sum_{K,V,C} \left| \langle \varphi_K^C | uxr | \varphi_K^V \rangle \right|^2$$

$$\times \delta\left(E_K^C - E_K^V - \hbar\omega\right), \tag{6}$$

TABLE II. Calculated values of the direct band gap of Al$_{0.50}$Ga$_{0.50}$N$_x$Sb$_{1-x}$ alloys obtained within GGA-PBEsol+mBJ approximation in comparison with experimental data and other theoretical values.

Compound	Eg(eV)
Al$_{0.50}$Ga$_{0.50}$N$_{0.125}$Sb$_{0.875}$	0.43872
Al$_{0.50}$Ga$_{0.50}$N$_{0.25}$Sb$_{0.75}$	0.00000
Al$_{0.50}$Ga$_{0.50}$N$_{0.75}$Sb$_{0.25}$	1.81838
Al$_{0.50}$Ga$_{0.50}$N$_{0.875}$Sb$_{0.125}$	2.30677

where ω is the frequency of the light, e is the electric charge is the vector defining the polarization of the incident electric field, Ω is the unit cell volume, φ_K^C and φ_K^V are the wave functions of the conduction and valence bands, respectively. The real part of the dielectric function $\varepsilon_1(\omega)$ is determined by employing the Kramers-Kronig [26, 27] relations expressed as follows:

$$\varepsilon_1(\omega) = 1 + \frac{2}{\pi} P \int_0^\infty \frac{\omega'\varepsilon_2(\omega')}{\omega'^2 - \omega^2} d\omega'. \tag{7}$$

Figure 8 shows the real part of the dielectric function for Al$_{0.50}$Ga$_{0.50}$N$_x$Sb$_{1-x}$. It is evident that the zero frequency limits $\varepsilon_1(0)$ is a fundamental parameter, which describes the dielectric response to the static electric field. The static dielectric constants of the Al$_{0.50}$Ga$_{0.50}$N$_x$Sb$_{1-x}$ alloys at considered Nitrogen (N) concentrations (x = 0.125, 0.25, 0.75, 0.875) are 568.668, 601.714, 158.032, and 142.251, respectively. We notice that the real part of the dielectric function $\varepsilon_1(\omega)$ for Al$_{0.50}$Ga$_{0.50}$N$_{0.125}$Sb$_{0.875}$, and Al$_{0.50}$Ga$_{0.50}$N$_{0.25}$Sb$_{0.75}$ becomes negative, from energy which is called plasma energy $E_p = \hbar\omega_p$, with $\hbar$ is reduced Planck constant, and ω_p is the plasma frequency. We have
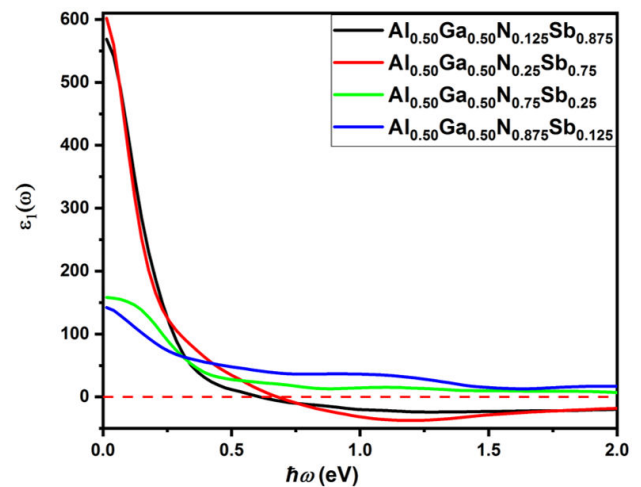
FIGURE 8. Calculated real parts of the dielectric function of Al$_{0.50}$Ga$_{0.50}$N$_x$Sb$_{1-x}$ structures.
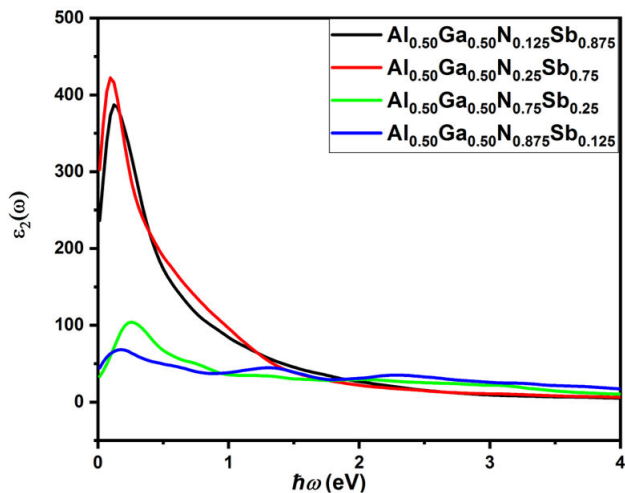
FIGURE 9. Calculated imaginary parts of the dielectric function of $Al_{0.50}Ga_{0.50}N_xSb_{1-x}$ structures.
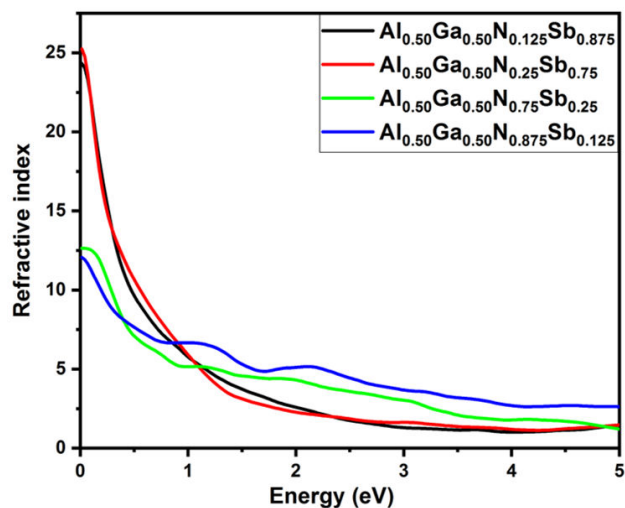
FIGURE 10. The refractive index $n(\omega)$ of $Al_{0.50}Ga_{0.50}N_xSb_{1-x}$ structures.

found the plasma energy at 0.61093 eV and 0.67841 eV for $x = 0.125$ and 0.25, respectively. In addition to that, the energy plasma is the energy where the material becomes conductive (metallic comportment) [24-28]; according to our calculation, it is reasonable because their bandgap is 0.43872 and 0.0000 eV, respectively. Furthermore, the curves are grouped in pairs, for concentration (0.125, 0.25) and (0.75, 0.875), which have almost the same contour and may be for their nearby bandgap. The imaginary part of the dielectric function (absorptive) for $Al_{0.50}Ga_{0.50}N_xSb_{1-x}$ is represented by Fig. 9. It is apparent that the imaginary part of the dielectric function exhibits various comportments for different compositions x, with different peaks located at 0.12245, 0.09524, 0.25851, and 0.17687 eV, for $x = 0.125$, 0.25, 0.75, and 0.875, respectively. The imaginary part of dielectric amplitude (ε_2) is inversely proportional to the bandgap. The lowest gap is 0, 0.43872, 1.81838, and 2.30677 eV for the structures $Al_{0.50}Ga_{0.50}N_{0.25}Sb_{0.75}$

(red curve), $Al_{0.50}Ga_{0.50}N_{0.125}Sb_{0.875}$ (black curve), $Al_{0.50}Ga_{0.50}N_{0.75}Sb_{0.25}$ (green curve), and $Al_{0.50}Ga_{0.50}N_{0.875}Sb_{0.125}$ (blue curve), respectively. The peak (high value) of the imaginary part of the dielectric function of different structures is located at 0 and 0.5 eV, which can be due to the crystal structure which is almost identical (if we neglect the radius of N in front of Sb). The associate of the real and imaginary parts of the dielectric function allowance the calculation of fundamental optical properties such as the refractive index $n(\omega)$, extinction coefficient $K(\omega)$, and the optical conductivity $\sigma(\omega)$ [29-31]. The refractive index $n(\omega)$, extinction coefficient $K(\omega)$, and the optical conductivity $\sigma(\omega)$ are calculated from the Eqs. (8), (9) and (10), respectively.

$$n(\omega) = \frac{1}{\sqrt{2}}[(\varepsilon_1^2(\omega) + \varepsilon_2^2(\omega))^{1/2} + \varepsilon_1(\omega)]^{1/2} \quad (8)$$

$$K(\omega) = \frac{1}{\sqrt{2}}[(\varepsilon_1^2(\omega) + \varepsilon_2^2(\omega))^{1/2} - \varepsilon_1(\omega)]^{1/2} \quad (9)$$

$$\sigma(\omega) = \frac{N_e e^2}{m_{eff}} \frac{\omega'}{\omega^2 - \omega'^2} \quad (10)$$

The refractive index is a fundamental optical constant. It can present data about the comportment of light in materials; when light passes through the different structures, its velocity decreases by increasing the refractive index of these structures [32]. Figure 10 represents the refractive index versus light energy (spectral radiations). The maximum refractive index for $Al_{0.50}Ga_{0.50}N_xSb_{1-x}$ for all concentrations is situated at zero frequency limits, the static refractive index $n(0)$ for $x = 0.125$, 0.25, 0.75, and 0.875 are around 24.3361, 25.2517, 12.6392 and 12.0682 eV, respectively, and is decreased as a function of energy. The extinction coefficients of $Al_{0.50}Ga_{0.50}N_xSb_{1-x}$ for different concentrations are presented in Fig. 11. We remark that the extinction coefficient increases and decreases after attaining a peak for all concentrations except for $x = 0.875$ composition. The peaks located at
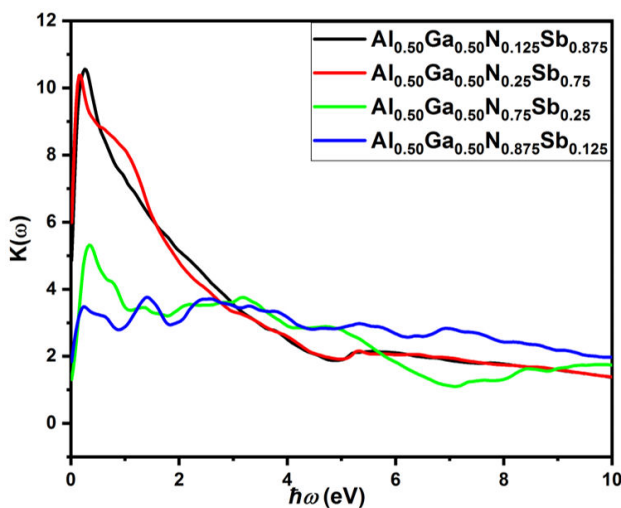
FIGURE 11. Extinction coefficient $K(\omega)$ for $Al_{0.50}Ga_{0.50}N_xSb_{1-x}$ structures.
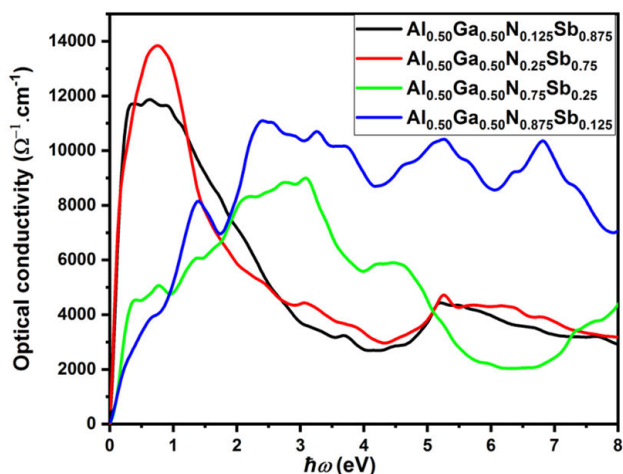
FIGURE 12. Optical conductivity of Al$_{0.50}$Ga$_{0.50}$N$_x$Sb$_{1-x}$ structures.

0.25851, 0.14966, and 0.34014 eV for $x = 0.125$, 0.25, and 0.75, respectively, and several peaks for $x = 0.875$ situated at 0.23130, 1.40139 and 2.46263 eV. The plots of the optical conductivity $\sigma(x)$ within the GGA-PBEsol approach are displayed in Fig. 12. Various peaks are presented in the feature of $\sigma(x)$ curves, which are vary in agreement with the energy bandgap.

4. Conclusion

We have presented a theoretical study of the structural, electronic, and optical properties of Al$_{0.50}$Ga$_{0.50}$N$_x$Sb$_{1-x}$ alloys in the zincblende structure (B3) employing the FP-LAPW approach with the GGA-PBEsol and TB-mBJ approximation. We have found that all structures have a direct bandgap located at $\Gamma - \Gamma$ high-symmetry points except the Al$_{0.50}$Ga$_{0.50}$N$_{0.25}$Sb$_{0.75}$ alloy, which has a semi-metallic comportment. The real and imaginary parts of the dielectric function $\varepsilon_1(\omega)$, $\varepsilon_2(\omega)$, the refractive index $n(\omega)$, extinction coefficient $K(\omega)$ and the optical conductivity $\sigma(\omega)$ are determined. The curves are grouped in pairs, for concentration (0.125, 0.25) and (0.75, 0.875), which have almost the same contour, which may be for their nearby bandgap. Our results show that the Al$_{0.50}$Ga$_{0.50}$N$_x$Sb$_{1-x}$ structures for all concentrations except $x = 0.25$ are promising candidates for optoelectronic applications.

1. M. Benchehima and H. Abid, Electronic and optical properties of Al$_x$Ga$_y$In$_{1-x-y}$As quaternary alloys with and without relaxation lattice matched to InP for laser applications: First-principles study, *Optik* **127** (2016) 6541, https://doi.org/10.1016/j.ijleo.2016.04.092.

2. Y. Chen, P. Zhu, L. Wu, X. Chen and P. Lu, First-principles study on composition-dependent properties of quaternary InP$_{1-x-y}$N$_x$Bi$_y$ alloys, *Mod. Phys. Lett. B* **34** (2020) 2050111, https://doi.org/10.1142/S0217984920501110.

3. S. Das, A. S. Sharma, S. A. Gazi and S. Dhar, Growth of dilute quaternary alloy InPNBi and its? characterization, J. Cryst. Growth **535** (2020) 125532, https://doi.org/10.1016/j.jcrysgro.2020.125532

4. Y. Guan, G. Luo, D. Morgan, S. E. Babcock and T. F. Kuech, Thermodynamic stability analysis of Bi-containing III-V quaternary alloys and the effect of epitaxial strain, *J. Phys. Chem. Solids* **138** (2020) 109245. https://doi.org/10.1016/j.jpcs.2019.109245.

5. H. Saidi and S. Ridene, Design considerations of AlGaInAs quaternary nanowires for mid-infrared applications, *Chem. Phys. Lett.* **738** (2020) 136872. https://doi.org/10.1016/j.cplett.2019.136872

6. Y. Guan, A. Rajeev, S. E. Babcock, L. J. Mawst and T. F. Kuech, Metal-organic vapor phase epitaxy of the quaternary metastable alloy In$_{1-x}$Ga$_x$As$_{1-y}$Bi$_y$ and its kinetics of growth, *J. Cryst. Growth* (2020) 125611. https://doi.org/10.1016/j.jcrysgro.2020.125611.

7. H. Xie, H. Lin, Q. Xu, H. Lu, Y. Sun, S. Hu and N. Dai, Investigation of surface morphology of InAs$_{1-x-y}$Sb$_x$P$_y$ epilayers grown by liquid phase epitaxy, *J. Cryst. Growth* **534** (2020) 125464, https://doi.org/10.1016/j.jcrysgro.2019.125464.

8. W. Kohn and L. J. Sham, Self-Consistent Equations Including Exchange and Correlation Effects, *Phys. Rev.* **140** (1965) A1133. https://doi.org/10.1103/PhysRev.140.A1133.

9. P. Blaha, K. Schwarz, G. K. H. Madsen, D. Kvasnicka and J. Luitz, *An Augment. Pl. wave+ local orbitals Progr. Calc. Cryst. Prop.*

10. K. Schwarz, P. Blaha, and G. K. H. Madsen, Electronic structure calculations of solids using the WIEN2k package for material sciences, *Comput. Phys. Commun.* **147** (2002) 71, https://doi.org/10.1016/S0010-4655(02)00206-0.

11. G. K. H. Madsen, P. Blaha, K. Schwarz, E. Sjöstedt and L. Nordström, Efficient linearization of the augmented plane-wave method, *Phys. Rev. B* **64** (2001) 195134, https://doi.org/10.1103/PhysRevB.64.195134

12. J. P. Perdew, K. Burke, and M. Ernzerhof, Generalized Gradient Approximation Made Simple, *Phys. Rev. Lett.* **77** (1996) 3865. https://doi.org/10.1103/PhysRevLett.77.3865.

13. F. Tran and P. Blaha, Accurate Band Gaps of Semiconductors and Insulators with a Semilocal Exchange-Correlation Potential, *Phys. Rev. Lett.* **102** (2009) 226401. https://doi.org/10.1103/PhysRevLett.102.226401.

14. D. Koller, F. Tran and P. Blaha, Merits and limits of the modified Becke-Johnson exchange potential, *Phys. Rev. B* **83** (2011) 195134. https://doi.org/10.1103/PhysRevB.83.195134.

15. D. Koller, F. Tran and P. Blaha, Improving the modified Becke-Johnson exchange potential, *Phys. Rev. B* **85** (2012) 155109. https://doi.org/10.1103/PhysRevB.85.155109.

16. H. Jiang, Band gaps from the Tran-Blaha modified Becke-Johnson approach: A systematic investigation, *J. Chem. Phys.* **138** (2013) 134115. https://doi.org/10.1063/1.4798706.

17. S.-D. Guo and B.-G. Liu, Improved half-metallic ferromagnetism of transition-metal pnictides and chalcogenides calculated with a modified Becke-Johnson exchange potential, *EPL Europhysics Lett.* **93** (2011) 47006. https://doi.org/10.1209/0295-5075/93/47006.

18. S. W. Fan, L. J. Ding, Z. L. Wang and K. L. Yao, Half-metallic ferromagnetism in wurtzite ScM (M=C, Si, Ge, and Sn): Ab initio calculations, *Appl. Phys. Lett.* **102** (2013) 22404, https://doi.org/10.1063/1.4775680.

19. B. G. Yalcin, Structural, mechanical and thermodynamic properties of N-dope BBi compound under pressure, *Appl. Phys. A* **122** (2016) 456, https://doi.org/10.1007/s00339-016-0003-1

20. S. Bagci and B. G. Yalcin, Structural, mechanical, electronic and optical properties of BBi, BP and their ternary alloys $BBi_{1-x}P_x$, *J. Phys. D. Appl. Phys.* **48** (2015) 475304, https://doi.org/10.1088/0022-3727/48/47/475304.

21. B. G. Yalcin, Band gap characterization of ternary $BBi_{1-x}N_x$ $(0 \leq x \leq 1)$ alloys using modified Becke?Johnson (mBJ) potential, *Phys. B Condens. Matter* **462** (2015) 64, https://doi.org/10.1016/j.physb.2015.01.021.

22. F. Birch, Finite Elastic Strain of Cubic Crystals, *Phys. Rev.* **71** (1947) 809, https://doi.org/10.1103/PhysRev.71.809.

23. L. Vegard, Formation of Mixed Crystals by Solid-Phase Contact, *J. Phys.* **5** (1921) 393. doi: 10.1007/BF01327675

24. K. W. Wong and S. C. Lo, Conditions for the existence of a mixed superconducting and excitonic phase in Semimetals, *Phys. Lett. A* **31** (1970) 260, https://doi.org/10.1016/0375-9601(70)90961-8.

25. H. A. Donfack, Electronic and Optical Properties of Silicon-Germanium-Tin alloys, (Arizona State University, 2011) .

26. R. de L. Kronig, On the Theory of Dispersion of X-Rays, *Josa* **12** (1926) 547. https://doi.org/10.1364/JOSA.12.000547.

27. H. A. Kramers, *in Atti Cong. Intern. Fisica* (Transactions of Volta Centenary Congress) Como, **2** (1927) 545.

28. H. Ehrenreich and M. H. Cohen, Self-Consistent Field Approach to the Many-Electron Problem, *Phys. Rev.* **115** (1959) 786, https://doi.org/10.1103/PhysRev.115.786.

29. M. Dressel, G. Grüner, J. E. Eldridgec and J. M.Williamsd, Optical properties of organic superconductors, *Synthetic Metals* **70** (1997) 1503, https://doi.org/10.1016/S0379-6779(97)80325-6.

30. M. Fox, Optical Properties of Solids, *Amer. Jour. Phys.* **70** (2002) 1269. https://doi.org/10.1119/1.1516200.

31. D. R. Penn, Wave-Number-Dependent Dielectric Function of Semiconductors, *Phys. Rev.* **128** (1962) 2093. https://doi.org/10.1103/PhysRev.128.2093.

32. M. Hadjab, S. Berrah, H. Abid, M. I. Ziane, H. Bennacer and A. H. Reshak, First-principles investigation of the optical properties for rocksalt mixed metal oxide $Mg_xZn_{1-x}O$, *Mater. Chem. Phys.* **182** (2016) 182. https://doi.org/10.1016/j.matchemphys.2016.07.021.